Available online at www.sciencedirect.com

SCIENCE DIRECT®

Journal of Volcanology and Geothermal Research 148 (2005) 334–354

Journal of volcanology and geothermal research

www.elsevier.com/locate/jvolgeores

Relative partitioning of acoustic and seismic energy during Strombolian eruptions

J.B. Johnson[a,*], R.C. Aster[b]

[a]Department of Earth Sciences, University of New Hampshire, NH 03824, United States

[b]Department of Earth and Environmental Science and Geophysical Research Center, New Mexico Tech, Socorro, NM 87801, United States

Received 17 May 2004; received in revised form 23 March 2005; accepted 22 May 2005

Abstract

The relative elastic energy partitioning during Strombolian eruptions can be estimated from acoustic pressure and seismic velocity records. We outline methods for determining acoustic and seismic energies for sensors deployed within several kilometers of erupting vents. We use these energies to introduce the concept of the volcano acoustic–seismic ratio (η, or VASR), which is the ratio of elastic energy propagated through the atmosphere and into the earth. Eruption VASR is a physical diagnostic of explosive degassing that is appropriate for comparing eruption mechanisms at individual and between various volcanoes. Here we assess acoustic and seismic energies and corresponding VASR for discrete Strombolian explosive events at Karymsky and Erebus Volcanoes. We attribute the relatively high and stable VASR at Erebus ($\eta = 8$, standard deviation 41%) to repeatable source conditions occurring at the surface of a persistent lava lake, with accompanying strong coupling to the atmosphere. Lower and more variable VASR at Karymsky ($\eta = 0.18$ in 1998 to $\eta = 1.51$ in 1991, with standard deviations of 93% and 313%, respectively) is attributed to changing conditions within a narrow, partially choked conduit. Variable seismo-acoustic energy partitioning for Karymsky, as manifested by the large VASR standard deviation, suggests that conduit conditions affecting VASR, which include magma properties, conduit obstruction, or fragmentation depths can evolve both during the course of an explosion and between successive events.

Keywords: volcano seismology; volcanic infrasound; Karymsky; Erebus; energy partitioning

1. Introduction

Researchers at several active volcanoes, including Langila (Mori et al., 1989), Arenal (Garces et al., 1998a; Hagerty et al., 2000), Erebus (Aster et al., 2003; Johnson et al., 2003; Rowe et al., 2000), Stromboli (Ripepe et al., 1993), Karymsky (Johnson and Lees, 2000) and Shishaldin (Caplan-Auerbach and McNutt, 2003), have noted widely variable partitioning of seismic energy propagated into the ground and acoustic energy propagated into the atmosphere. This variability has been attributed primarily to source or near-source-related phenomena as

* Corresponding author. Tel.: +1 808 956 3149.
E-mail address: jeff.johnson@unh.edu (J.B. Johnson).

0377-0273/$ - see front matter © 2005 Elsevier B.V. All rights reserved.
doi:10.1016/j.jvolgeores.2005.05.002

opposed to time-varying earth or atmospheric propagation effects. Here we discuss some general issues affecting this elastic energy partitioning using data collected at two Strombolian-type volcanoes, Karymksy in Russia and Erebus in Antarctica. These volcanoes have been selected because of the existence of quality seismo-acoustic data for a large suite of discrete explosive events.

The first volcano, Karymsky, is the most active volcano of Kamchatka's eastern volcanic zone and has generated both Strombolian and Vulcanian activity in recent decades. Most of the symmetric 800-m-tall andesitic edifice has been constructed within the last 2000 years (Ivanov et al., 1991). Since 1996, Karymsky has been persistently in eruption, producing ash and ballistic-rich Strombolian-type explosive events 5 to 20 times each hour (Johnson and Lees, 2000) and occasional block lava flows which have reached the base of the cone.

The second volcano, Erebus, is another persistently active Strombolian-type volcanic system located on Ross Island, Antarctica (Kyle, 1994). For at least several decades Erebus has maintained an exposed conduit in its inner crater, which appears as a small (up to 40-m-diameter) lava lake of phonolitic composition (Dibble, 1994). Strombolian-type eruptions at Erebus are readily seen in video records corresponding to the intact delivery of single, or occasionally multiple, slugs of gas with diameters of up to ~7 m (Aster et al., 2003; Rowe et al., 2000).

Simultaneous and co-located infrasonic and seismic data have been collected at both Erebus and Karymsky for several field seasons, with seismometers and acquisition systems loaned by the Program for Array Seismic Studies of the Continental Lithosphere (PASSCAL). The infrasonic sensors have been designed and constructed with help from Pat McChesney of the University of Washington (Johnson et al., 2003). Fig. 1 provides deployment maps for the seismo-acoustic installations used in these studies. Data presented here come from campaign-style experiments conducted in Dec–Jan. of 2000–2001 (Erebus) and September 1998 and 1999 (Karymsky). During these experiments explosions occurred at Erebus on average several times each day and at Karymsky on average 5 to 20 times each hour.

In principle, the relative elastic energies of acoustic and seismic wavefields may be quantified from seismic ground motion and infrasonic pressure data and used to provide physical constraints and general insight into fundamental aspects of volcano degassing. Here we explore how relative energy partitioning may be strongly controlled by the geometry of the conduit/vent system, the volatile and multiphase characteristics of the magma, the physical dimensions of the source, and the extent to which the system is disrupted. Although apparent variations in seismo-acoustic energy partitioning may also be caused by changing atmospheric conditions (Pierce, 1981), explosive events at volcanoes, such as those at Karymsky (Johnson, 2000) and Arenal (Hagerty et al., 2000), demonstrate systematically variable seismo-acoustic energy partitioning over time scales of only a few tens of seconds. These variations are too rapid to be attributed to changing weather (i.e., atmospheric propagation effects).

Although elastic energy comprises only a few percent of the total energy budget transferred during explosive eruptions (McGetchin and Chouet, 1979), radiated seismic and acoustic signals present convenient observables for quantifying eruption conditions and intensity. Most infrasonic microphones currently used for volcano monitoring are capable of reliably recording high-amplitude pressure perturbations in the near-infrasound range (several seconds to 20 Hz) (Johnson et al., 2003). This is the bandwidth that appears to contain the highest spectral energy density for atmospheric airwaves due to small and moderate-sized volcanic eruptions (Johnson et al., 2004; M. Garces pers. comm., 2003; Vergniolle and Brandeis, 1994). In the analysis presented here we acknowledge that the frequency response of our microphones (low-end corner frequency from 0.27 to ~4.5 Hz) may be somewhat limiting. However, we contend that consistent recording of the eruptions with similar microphones permits robust acoustic energy comparisons. We do not attempt to quantify the absolute acoustic efficiency (ratio of acoustic energy to explosive yield) for these eruptive events.

For seismic energy, the frequency response of portable broadband seismometers, such as those used in our campaigns, is adequate to record both high-frequency (to tens of Hz) ground motions as

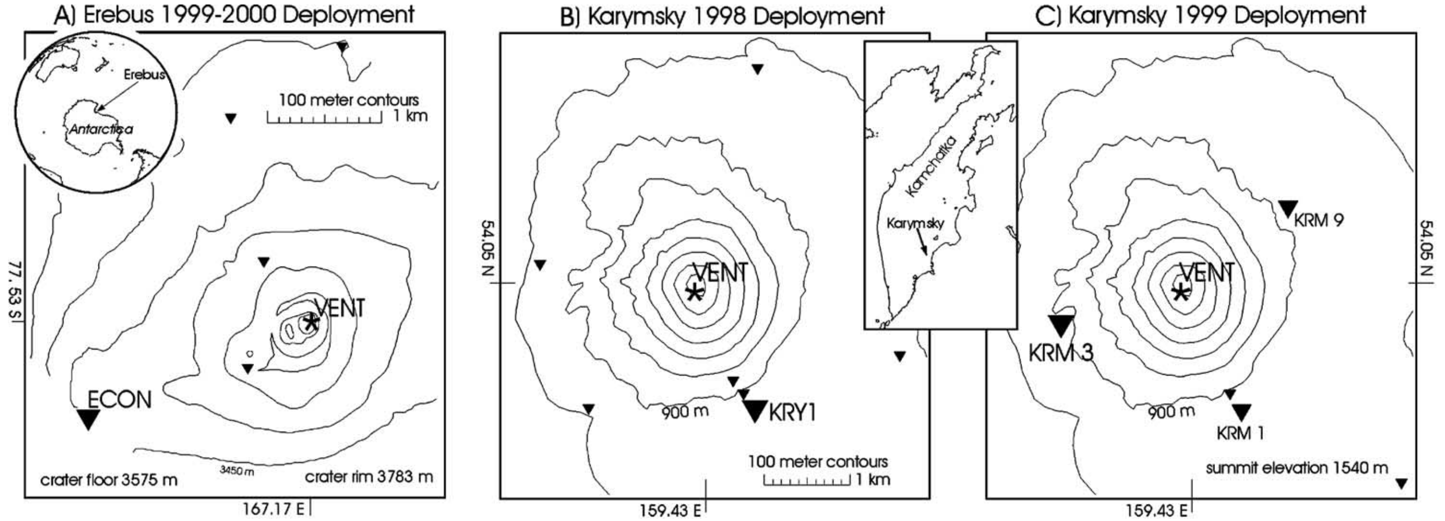

Fig. 1. Maps of seismo-acoustic sensor deployment at: A) Erebus and B–C) Karymsky Volcanoes (1998 and 1999). Inverted triangles indicate co-sited broadband seismometers and infrasonic microphones. Large triangles, marked ECON (2080 m from vent), KRY1 and KRM1 (1620 m from vent), KRM3 (1760 m from vent), and KRM9 (1820 m from vent), denote sensor sites for data used in this study.

well as very long period (VLP; 5 s and longer) energy associated with explosion earthquakes. Examples of erupting volcanoes with observed VLP events include Stromboli (Neuberg et al., 1994), Erebus (Aster et al., 2003), Popocatepetl (Arcineiga-Ceballos et al., 1999), and Merapi (Hidayat et al., 2002). VLP events have been successfully modeled in Strombolian systems as near-field signals caused by conduit system mass transport processes (e.g., Chouet et al., 1997). However, their energy content, compared to the high-frequency bandwidth, is generally very low and does not significantly increase seismic energy estimates.

2. Estimation of acoustic energy

Acoustic energy radiated during volcanic eruptions is relatively straightforward to evaluate from infrasonic pressure traces under simplifying assumptions. Atmospheric infrasound propagates with a relatively fixed velocity, ranging from 306 m/s at -40 °C to 355 m/s at 40 °C. For large eruptions in excess of Volcano Explosivity Index 3 (VEI) (Newhall and Self, 1982), such as Mount St. Helens (Mikumo and Bolt, 1985) and Pinatubo (Tahira et al., 1996), significant atmospheric gravity waves with periods of hundreds of seconds may also be excited. However, high-intensity gravity waves are not observed for small-scale Strombolian and Vulcanian activity. Here we present and analyze data from very small (VEI 0–1), discrete eruptive events recorded across multi-element infrasound networks that have been installed within a few kilometers of the vent. At these distances, infrasound is well correlated across network elements, appears non-dispersive, and suffers negligible source–receiver intrinsic attenuation e.g., (Bedard and Georges, 2000). A more detailed description of the deployed microphone networks (Fig. 1), which included 3 and 5 microphones during the Karymsky experiments and 6 microphones at Erebus, is given in Johnson et al. (2003).

Low-amplitude infrasound propagates with an energy density that is proportional to the square of the excess pressure (ΔP) divided by the air density (ρ_{atmos}) and sound speed (c_{atmos}) (Pierce, 1981). Assuming isotropic radiation, as from a point source monopole, we can space–time integrate over a hemispherical surface to estimate the total acoustic energy radiated into the atmosphere e.g., (Firstov and Kravchenko, 1996; Johnson, 2003; Vergniolle et al., 2004):

$$E_{\mathrm{acoustic}} = \frac{2\pi\ r^2}{\rho_{\mathrm{atmos}} c_{\mathrm{atmos}}} \int \Delta P(t)^2 dt \tag{1}$$

To characterize the acoustic energy corresponding to discrete Strombolian explosive events, we integrate over a time window spanning the entire duration of the acoustic transient. The integral is thus calculated from the signal onset until the time when both seismic and acoustic amplitudes have decayed to background levels.

It is important to note that Eq. (1) assumes linear sound propagation (infinitesimal excess pressure with respect to ambient pressure), but non-linear propagation is conceivable in the near field for very energetic explosions (Myagkov, 1998; Raspet, 1998; Reed, 1987). For non-linear pressure disturbances, radial propagation will not yield a simple inverse relationship between distance and excess pressure (Kinney and Graham, 1985). In this situation, viscous and molecular heat dissipation induce a rapidly decaying acoustic pressure, invalidating Eq. (1) at distances less than the linear elasticity radius. For intense eruptions, non-linear atmospheric propagation may then result in underestimation of the explosive source energy imparted to the atmosphere. It is also important to note that Eq. (1) assumes a monopole source. Non-monopole volcano acoustic sources have been proposed by Woulff and McGetchin (1975).

Sound velocity anisotropy in the atmosphere is another potential complication because inhomogeneous temperature and wind structure can very significantly refract acoustic energy (e.g., Garces et al., 1998b; Pierce, 1981; Reed, 1987). At distances greater than a few kilometers, these effects can cause excess pressure amplitude to be diminished by several orders of magnitude or even induce acoustic shadow zones (Reed, 1987). In these circumstances acoustic energy estimates would invariably need to incorporate more detailed acoustic propagation modeling. Nevertheless, isotropic radiation may be suitable in many cases for microphones deployed within a few kilometers of the vent. For instance, during typical recording conditions at Karymsky and Erebus, the maximum peak-to-peak infrasonic pressure amplitudes across the microphone networks did not vary by more than a factor of ~2 within 2.5 km of the vent (Johnson, 2000; Johnson et al., 2003). In practice, gain corrections may be applied as weather-dependent site responses for acoustic pressure sensors.

Acoustic and seismic background noise is nonlinearly correlated with wind speed (Hedlin et al., 1999; Withers et al., 1996) and represents a perpetual problem especially at volcanic infrasound installations. Array design and wind filters can minimize, but not eliminate broadband wind noise (Hedlin and Berger, 2002; Olson and Wilson, 1999). Nevertheless, it is usually feasible via spectral analysis and multidisciplinary correlation (e.g., with seismic, video, and microphone arrays/networks) to easily verify whether infrasonic pressure transients should be attributed to volcanic processes or to pulses of wind. For the acoustic energy calculations presented in this manuscript, we have taken care to select only low wind noise acoustic data.

Finally, the limited frequency response of microphones may influence estimates for acoustic energy calculated from raw data. This is not a significant issue when comparing energy estimates for a suite of explosions at a single instrument, assuming a linear system. However, the finite bandwidth must be accounted for during the comparison of suites of explosions recorded with a variety of different microphones. Thus, for our data, known transfer functions have been applied to the raw acoustic trace data. For example, such an adjustment to extend the effective corner frequency of the ECON microphone (from a single pole corner frequency originally at ~4.5 Hz to one at 0.25 Hz) accounts for an approximate threefold increase in acoustic energy values calculated at this station. At Karymsky an approximate 1.05, 1.05, and 1.8 factor increase in acoustic energy is registered at KRY1 (corner at 0.27 Hz), KRM3 (corner at 0.27 Hz), and KRM1 (corner at ~2.5 Hz). These energy scaling factors vary only slightly for different acoustic waveforms depending upon the frequency content of the infrasound. For the infrasonic data presented in this paper, frequency responses and microphone sensitivities (ranging from 42 to 200 mV/Pa) were both determined in a calibration chamber utilizing an absolute pressure transducer with known sensitivity and flat response.

3. Estimation of seismic energy

Radiated seismic energy is more difficult to estimate than the radiated infrasonic energy because the elastic propagation Green's functions are considerably more complex, particularly in the complicated impedance structures common in volcanic systems. An additional complication is that the seismic field includes P and S body waves as well as surface waves. Furthermore, strong seismic site responses created by near-surface conditions are common (e.g., Ruiz, 2003). Acknowledging these difficulties, we adopt an approach that assumes velocity waveforms are representative of the seismic kinetic energy density at a specific location on the volcano. Due to equipartitioning, potential energy density is equivalent to the kinetic energy density. Thus the total seismic energy is proportional to the product of the volcano density (ρ_{earth}) and the squared particle velocity (U^2) integrated over the volcano volume. An elastic energy equation analogous to Eq. (1), for an isotropic source located at the top of a homogeneous half space can be written as (e.g., Boatwright, 1980):

$$E_{\text{seismic}} = 2\pi r^2 \rho_{\text{earth}} c_{\text{earth}} \frac{1}{A} \int S^2 \; U(t)^2 dt \tag{2}$$

This equation incorporates corrections for seismic site response (S) and attenuation (A), which are fixed at unity for the datasets analyzed in this paper. To characterize the seismic energy associated with a discrete Strombolian event, we integrate over a time window that corresponds to the entire duration of the seismic transient. The integral is thus calculated from the signal onset until the time when seismicity returns to background levels. This interval may include several discrete pulses as well as extended-duration tremor-like signal, but it provides a standardized method for comparing discrete explosive events. For the data presented in this paper, velocity traces were primarily analyzed within a wide bandwidth of interest (0.5 to 12 Hz) to remove microseism noise and potential VLP contributions, and to match the infrasound bandwidth. Instrument sensitivities at Erebus (Guralp CMG-3 ESP seismometers) were 2000 V/m/s and at Karymsky (Guralp CMG-40 T seismometers) were 800 V/m/s.

Aside from site response uncertainty (unconstrained S), errors associated with Eq. (2) will arise from: 1) the treatment of seismic velocity traces as pure body waves, 2) the assumption of radial, isotropic seismic radiation, 3) assumption of negligible attenuation, and 4) the assignment of a single fixed P-wave wave velocity (c_{earth}).

We adopt assumption #1 and 4 for processing simplicity and because reduced displacement amplitudes (Aki and Koyanagi, 1981; Fehler, 1983; McNutt, 1994) recorded across the network of stations at Erebus show a better fit for body wave estimates than for surface wave estimates (Johnson, 2000). However we acknowledge that ground motions produced during volcanic eruptions are a complex amalgamation of wave types and scattered energy. To properly identify and differentiate the contributions from body and surface waves produced during volcanic eruptions multi-element seismic arrays should be utilized. For instance, a ~100-element seismic array at Stromboli Volcano, a potential analog for Karymsky and Erebus, indicated that body waves dominate between 0.5 to 2.5 Hz and surface waves dominate at higher frequencies (for a sensor array located a comparable distance ~1.7 km from the vent) (Chouet et al., 1998). At another volcano, Masaya, shallow source seismic tremor radiation was found to be dominated by body waves at close offsets (<1.5 km) and by surface waves at further offsets Metaxian et al. (1997).

Scattering of seismic energy invites further error because Eq. (2) assumes radial propagation. Assumption #2 is only appropriate if the scatterers are located relatively close to the source (Hellweg, 2000). Ideally, non-radially propagating seismic wavefield components should have their corresponding apparent wave speeds suitably reduced. Although seismic scattering brings about this complication, it also acts as a homogenizing influence in time-averaged observations because it compensates for azimuthal variations caused by source directivity, anisotropy, and/or inhomogeneous structures. To encourage tractable seismic energy estimates, we consistently process the Karymsky and Erebus seismograms assuming a predominance of compressional body waves, with the bulk of the energy propagating radially away from the explosion source. This is consistent with the analysis of eruption signals at Erebus by Dibble (1994) which suggested that explosion seismic signals were dominated by leaky trapped P-waves in the conduit system. Because our energy estimates therefore correspond to a P-wave-dominated seismic wavefield, they should be strictly considered upper bounds. The seismic energy content will be overestimated if there is a large surface wave component, if energy is not propagating radially outwards, or if body wave velocity is overestimated. Confirmation of isotropic radiation and wave type can be ideally realized through deployment of seismometer networks at various distances and azimuths from the seismic source. Experiments conducted at Piton de la Fournaise indeed show clear radial amplitude decay patterns with little azimuthal dependence (Aki and Ferrazzini, 2000). The geometric amplitude decay for body waves is sufficiently predictable that it can be used to locate source epicenters at this volcano, including long period events, tremor, and rockfall (Battaglia and Aki, 2003).

Radiated seismic energy will dissipate due to both intrinsic attenuation and scattering (e.g., Del Pezzo et al., 2001). For the data presented here, which is recorded at sites less than 2.1 km from the vents, we assume this dissipation to be small. However, proper assessment of attenuative energy loss will be necessary for seismic stations located further from the vent. Not accounting for geometric spreading, the attenuation of a wave may be expressed by $A(r) = \mathrm{e}^{(-\pi f r)/(c_{\mathrm{earth}} Q)}$, where f is the wave frequency and Q is a quality factor often determined from experimental data (Aki and Richards, 1980). Quality factors recovered at Etna and Masaya are frequency dependent (i.e., $Q = 10$ at $f = 2$ Hz) (Del Pezzo et al., 2001; Metaxian et al., 1997). Applying typical Q values recovered from these volcanoes, we discover that omission of attenuation will not likely diminish our seismic energy estimates by more than a factor of 1.3 for the furthest station used in the study (ECON, 2080 m from the Erebus vent).

Finally, we note that the seismicity may be contaminated by additional source processes, internal or external to the volcano, that may not be directly associated with an eruption. VLP signals at Erebus, for instance, precede the fragmentation event by several seconds and are attributed to buoyancy, reaction force, and gravitational disequilibrium processes associated with mass transport (Aster et al., 2003). For the purpose of seismic energy calculations at Erebus, this VLP seismicity often has only a small energy contribution due to its corresponding low velocity amplitude. For similar reasons, we attempt to disregard the potential seismic contributions caused by ground-coupled atmospheric airwaves. These high-frequency signals are commonly observed during Strombolian-type eruptions (e.g., Ripepe et al., 2001), but have low energy content in the Karymsky and Erebus datasets. Ground-coupled airwaves are generally evident only in seismic waveforms that have been high-pass filtered (above 4 Hz) and even when so filtered comprise only a few percent of the total waveform energy.

4. The Volcanic Acoustic–Seismic Ratio (VASR)

Using estimates of both acoustic energy (E_A) and seismic energy (E_S), we can characterize the relative partitioning of elastic energy into the atmosphere and into the solid earth by introducing a volcanic acoustic–seismic ratio (VASR):

$$\eta = \frac{E_A}{E_S} \tag{3}$$

VASR is a non-dimensional parameter that may provide insight into the evolving eruption source, magma characteristics, or conduit geometry for explosive eruptions. It can be calculated for either the entire duration of a discrete explosive event (as presented in this paper) or as a time-varying quantity for extended-duration events. VASR offers potential to facilitate the inter-comparison of explosive behavior at different volcanoes and to examine changing conditions within a suite of explosive events at a single volcano. Fig. 2 illustrates VASR alongside acoustic and seismic energy estimates for examples of discrete explosive events at Erebus and Karymsky. In these analyses, and in subsequent figures, acoustic and seismic energies have been calculated from calibrated acoustic and seismic waveforms that have been band-pass filtered between 0.5 and 12 Hz. Additional parameters used in our energy calculations are: ρ_{atmos} (1.2 kg/m^3), c_{atmos} (340 m/s), ρ_{earth} (2000 kg/m^3), and c_{earth} (2500 m/s). Fig. 2C demonstrates the temporally variable nature of VASR during an extended-duration degassing event at Karymsky. Although a composite VASR is calculated for this event using a 120-s window, it is readily apparent that if the two pulses were separated into two separate discrete events (indicated by the thick gray lines in Fig. 2C), they would indicate dramatically different energy partitioning occurring over very short time scales (~60 s). The rapid changes in VASR suggest that the variations are source-related and not due to changeable atmospheric structure, which presumably occurs over longer time scales. For certain long-duration events, it may be illustrative to calculate VASR for successive time windows to examine the time evolution of acoustic/seismic coupling.

Because VASR is sensitive to estimates of both seismic and acoustic energy, it is important to consider possible errors associated with each energy calculation. In the previous two sections, we outlined the primary assumptions associated with energy calculations. For the acoustic wavefield, weather-dependent anisotropic propagation will introduce the most significant errors. An effective way to check for the severity of this effect is to have multiple microphones deployed at different azimuths and distances from the vent. Fig. 3A compares acoustic energy estimates for 42 events at Karymksy recorded at two microphones that were spatially separated by more than 2.5 km and 100° relative to the vent. During these time intervals, the plume was affected by generally low winds (estimated <10 m/s) and conditions at each recording site were relatively calm. For the broadband acoustic signals (0.5 to 12 Hz), average acoustic energy estimated at the two microphones varies by a factor of 1.2, which is very small compared to the overall scatter in VASR. Variations in calculated acoustic energy are more notable for the high-frequency (4 to 12 Hz) filtered acoustic signals. This is likely due to diminished signal-to-noise content of the high frequency energy, but may also be caused by site effects, which can preferentially filter shorter wavelengths.

For the seismic wavefield, uncertain site response, unconstrained attenuation, and possible variations in source radiation directionality, which could vary from event to event, likely all contribute to errors in the seismic energy calculations. Fig. 3B compares seismic energy estimates for the same 42 events at three seismometers (KRM1, KRM3, and KRM 9) situated on three different sides of the volcano (Fig. 1C). The low degree of scatter in Fig. 3B strongly suggests that preferential source radiation direction is small for these eruptive events. Furthermore, relative site responses are also shown to be small as evidenced by the linear appearance and near-unity slope of data points in Fig. 3B. On average, KRM1 energies are 0.5 times smaller than KRM3 energies and KRM9 energies are 1.3 times as large. Although site responses induced by localized

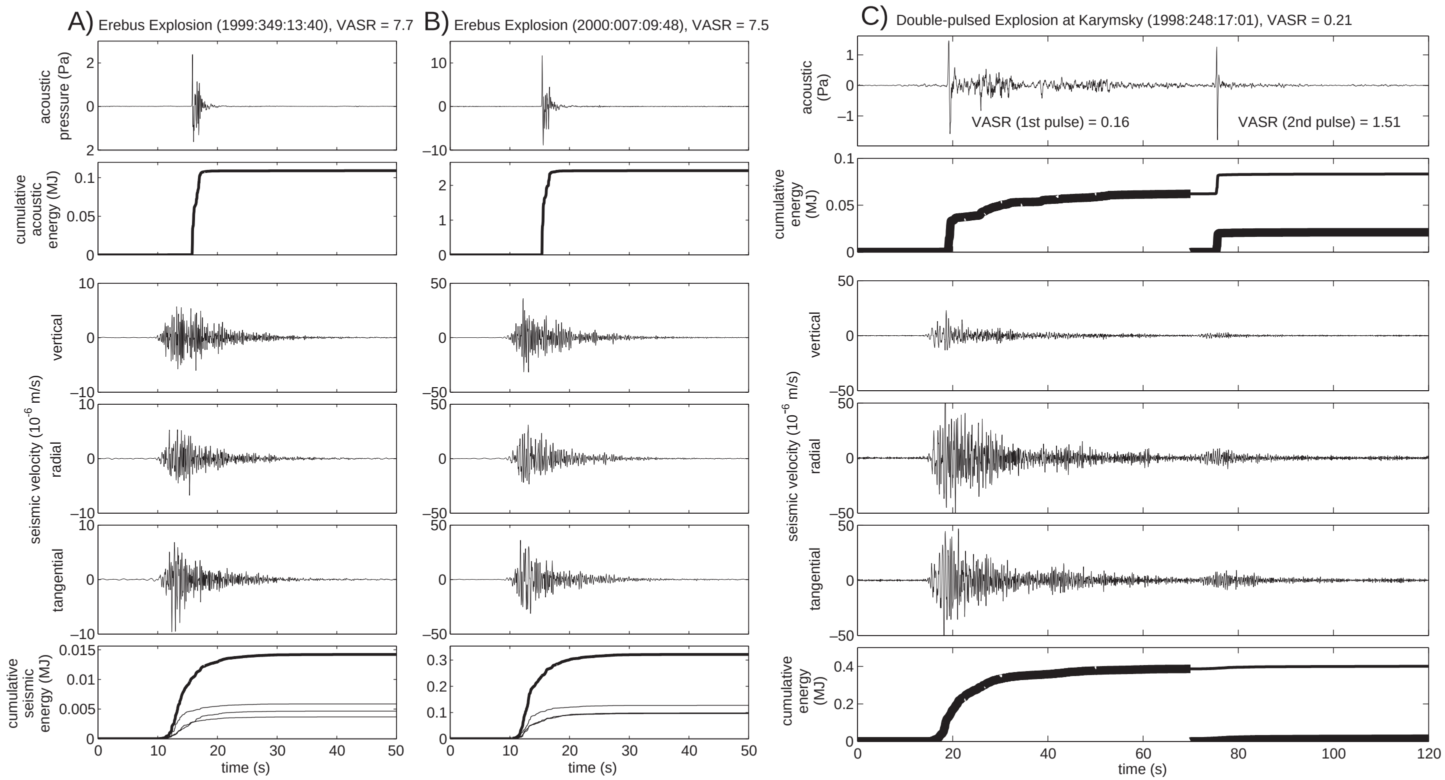

Fig. 2. A) Small and B) large Erebus explosive events tend to produce consistent volcano acoustic–seismic ratios ($\eta = 7.7$ and $\eta = 7.5$ calculated according to Eqs. (1), (2) and (3)). For each explosion, acoustic and three-component seismic traces are plotted along with the corresponding cumulative energy flux (from Eqs. (1) and (2)). VASR is the ratio of cumulative acoustic and seismic energy for an individual discrete event across an equivalent frequency band. C) Karymsky double-pulsed explosion demonstrating variable energy partitioning during a single event. The trace data depicted are characterized here as a single episode ($\eta = 0.21$), because seismic and acoustic amplitudes never drop to background levels between the two pulses. A dramatic increase in VASR ($\eta = 0.16$ and 1.51) is observed over a very short time interval (~60 s) when comparing the pulses individually.

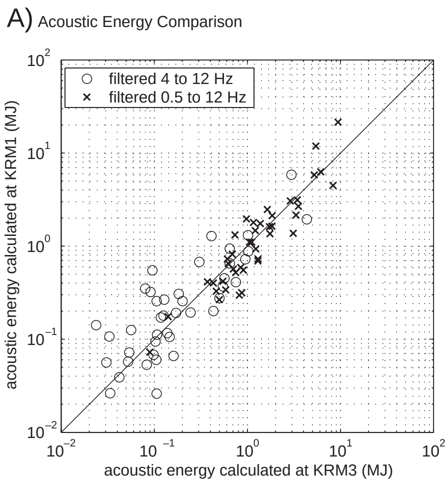

Fig. 3. Consistency of A) acoustic energies calculated at two different Karymsky stations in 1999 (Fig. 1C). Acoustic data are from KRM3 (1760 m) and KRM1 (1620 m) and include 42 low-noise events from Sep. 11–12. Station azimuthal orientation (relative to the vent) is ~100 degrees. Energies are calculated for broad and high-frequency bandwidths (0.5–12 and 4–12 Hz) and indicate poorer correlation for the higher frequency data. Calculated broadband acoustic energy values average 1.2 times as high at KRM3 compared to KRM1. B) Seismic energies calculated at three different Karymsky stations (Fig. 1C) corresponding to the same events. For the broadband seismic data, average energies are 0.5 times as high at KRM1 compared to KRM3 and 1.3 times as high at KRM9 (1820 m). In both plots, solid line is unity slope with zero intercept.

shallow structure may be substantial in certain cases (e.g., Mora et al., 2001), seismic site response variation in the studies at Karymksy or Erebus appear to affect VASR values by a factor of three or less this study.

Due to variable site responses, in which seismometer KRM3 appears about twice as sensitive as KRM1, the calculated average VASR (for the suite of 42 events at these two stations) differs by a factor

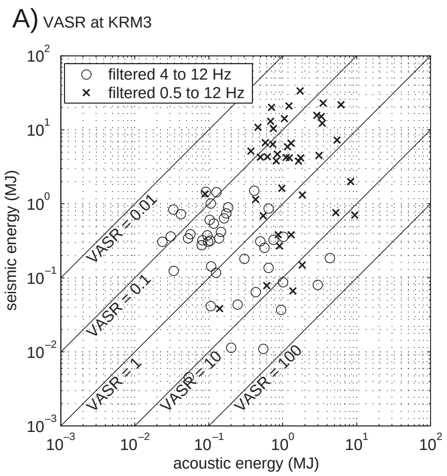

Fig. 4. VASR calculated for two different seismo-acoustic stations at Karymsky in 1999 (Fig. 1C). Data is from A) KRM3 (1760 m) and B) KRM1 (1620 m) and include 42 high signal-to-noise events from Sep. 11 and 12 (same events shown in Fig. 3). Azimuthal station separation (relative to the vent) is ~100 degrees (Fig. 1). VASR at both sites show comparable median values and scatter. Median energies are reduced by about one order of magnitude for the high-pass filtered data (4–12 Hz). Average VASR values for the broadband data are a factor of two greater for KRM1 than for KRM3 (η=2.2 and η=1.1). Variability in both panels is consistent and is significantly greater than the scatter in the consistency plots shown in Fig. 3, indicating that variable VASR at Karymsky is largely a source effects.

of 2 depending upon which station is used (Fig. 4). However, because the scatter in VASR values is comparable at both stations, we conclude that variable VASR is largely a reflection of variable source processes. It is also important to recall that seismic energy estimates (and corresponding VASR values) may be frequency dependent. Both Figs. 4 and 5 depict energy values for consistently filtered seismic and infrasound signals. For high-pass filtered signals (4–12 Hz), both acoustic and seismic energies appear to decrease by about an order of magnitude relative to the broad-band signals (0.5–12 Hz). If either acoustic or seismic traces are preferentially filtered, VASR values would also reflect the change. For this reason, we suggest that energies should be compared from signals, which are as broadband as possible, yet which exclude external noise (i.e., microseisms and wind).

Fig. 5 provides an overview of calculated VASR corresponding to discrete explosive events from suites of activity recorded at both Karymsky (1998 and 1999) and Erebus (1999–2000). Calculated VASR values for the Erebus dataset appears to remain relatively consistent despite three orders of magnitude variation in radiated total elastic energy. The general trend, which shows a correlated increase of both seismic and acoustic energies, is attributed to variations in explosive yield (eruption magnitude).

From data presented in Fig. 5, it is noteworthy that Erebus Volcano appears to radiate acoustic energy far more efficiently than Karymsky. Though caution must

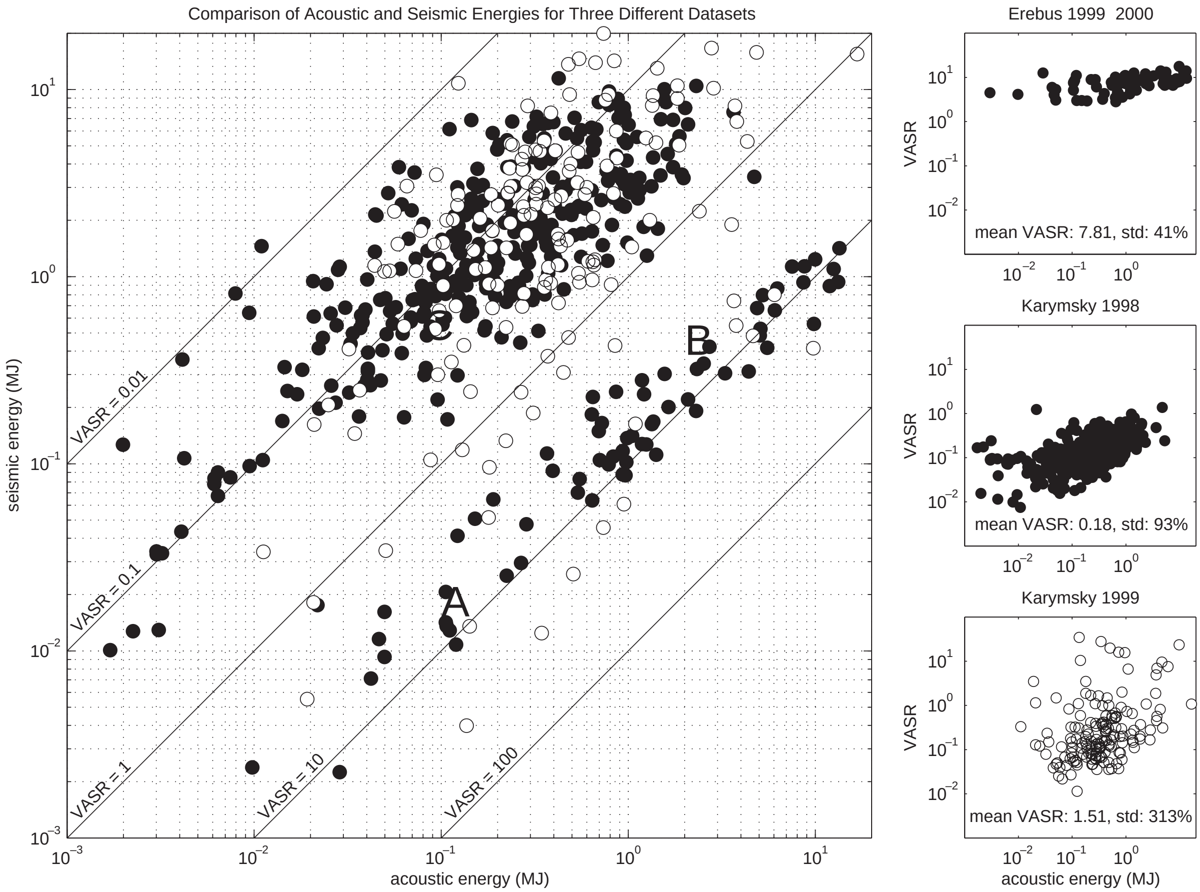

Fig. 5. Seismic and acoustic energies for 69 Erebus events (dark) recorded at ECON (2080 m from the vent), 344 Karymsky 1998 events (grey) recorded at KRY1 (1620 m from the vent), and 157 Karymsky 1999 events (white) recorded at KRM3 (1760 m from the vent). Individual events, indicated by A, B, and C, correspond to the examples shown in Fig. 2.

be practiced when comparing VASR from different volcanoes to assure that seismic energy estimates are not overtly biased by specific instrumentation or site responses, average Erebus VASR is found to be more than an order of magnitude greater than at Karymksy. Because the deployment conditions are similar (comparable epicentral distances and site conditions), we contend that the mean VASR for each dataset likely represents a systematic difference in eruption source conditions between the two volcanoes. This inference is supported by visual observations at both volcanoes. While Erebus explosions have been observed as bubble bursts rupturing the surface of a lava lake (Aster et al., 2003), Karymsky eruptions emanate from a scoria-choked conduit. The lack of blockage and corresponding acoustic shielding at the Erebus vent thus offers one possible explanation for the dramatic VASR difference.

The rightmost panels in Fig. 5 highlight VASR differences between the suites of explosions. While events at Erebus obey a relatively linear relation between radiated acoustic and seismic energies, Karymsky events display significant scatter, especially during 1999. The relatively consistent partitioning of seismo-acoustic energy at Erebus reflects highly repeatable, self-reconstructing source conditions (Aster et al., 2003; Johnson et al., 2003; Rowe et al., 2000, 1998), whereas variable VASR at Karymsky may conversely indicate changing conditions at or near the source.

5. Mechanisms for variable VASR

VASR variations have been inferred and interpreted at other active volcanoes. For example, Mori et al. (1989) examined explosive eruptions at Langila, Papua New Guinea, comparing seismic displacements with the amplitudes of associated air phases (acoustic airwaves coupled to the ground). They noticed significant variability in the ratio of seismic and acoustic amplitudes and proposed variable transferal of explosive energy into the mechanical energy required to blast dense material from the vent. Ripepe et al. (1993) observed that the ash-rich explosive eruptions at Stromboli, Italy were generally associated with relatively low amplitude seismic signals and proposed that less ground shaking occurs during a well-formed vertical eruption because less ejecta momentum is imparted laterally to the wall rocks. Garces et al. (1998a) argued that variable seismo-acoustic partitioning at Arenal, Costa Rica, could be explained by time-varying melt properties which dramatically affect impedance contrasts. Rowe et al. (2000) employed a similar mechanism to explain the variations in seismic/acoustic partitioning for the smallest explosions at Erebus, where very small superficial bubble bursts may be seismically isolated from the high impedance wall rock and/or deeper portions of the lava lake. Thompson et al. (2002) and Caplan-Auerbach and McNutt (2003) investigated acoustic waves associated with both Plinian and Strombolian eruptions at Shishaldin and associated larger acoustic signals with later eruptive stages when both the vent and conduit were relatively open (S. McNutt pers. comm., 2000).

Systematic explanations for variable VASR in various eruptive systems are presently speculative, but have potential merit for improving understanding of eruptive processes. We next quantify simplified versions of some of these models to explain the observed VASR temporal variability at Karymsky Volcano and general differences between Karymsky and Erebus. For each eruptive process we consider that potential energy from pressurized volatiles is transmitted into the surrounding media (atmosphere and volcano) as elastic energy. Additional potential energy contributions, due to accumulated gravitational or elastic strain, are neglected in this simplified energy budget analysis. For the adiabatic, isentropic expansion of pressurized gases ($P_{\mathrm{initial}} \rightarrow P_{\mathrm{final}}$), the total available potential energy (explosive yield) can be calculated using Kinney and Graham (1985):

$$E_{\mathrm{explosion}} = \frac{M}{m}\frac{RT_{\mathrm{initial}}}{\gamma - 1}\left(1 - \left(\frac{P_{\mathrm{final}}}{P_{\mathrm{initial}}}\right)^{\frac{\gamma-1}{\gamma}}\right) \approx 5 \times 10^{6} M\left(1 - \left(\frac{P_{\mathrm{final}}}{P_{\mathrm{initial}}}\right)^{0.1}\right) \quad (4)$$

where M is the mass of volatiles, m is the volatile molecular weight (0.018 kg/mole for water vapor), R is the gas constant (8.314 J/mol/Kelvin), T_{initial} is the compressed gas temperature (1000 °C for magmatic volatiles), and γ is the heat capacity ratio (fixed at 1.1 for hot gases).

During volcanic eruptions, the conversion of potential energy stored as pressurized gas to elastic energy in the form of seismic and acoustic waves is expected to be a highly inefficient process. At Karymsky and Erebus, the measured elastic energy (according to Eqs. (1) and (2)) is several orders of magnitude smaller than the yield for an expected explosive outflux of thousands of kilograms of compressed gas (Fig. 6). This inefficiency is comparable to that of tectonic earthquakes, where radiated seismic energy is typically only a few percent or less of the total energy budget (e.g., Dobrovol'skiy, 1994; Duvall and Stephenson, 1965). During volcanic eruptions, the vast majority of energy is thought to be lost through heat transfer, as kinetic energy imparted to erupted products, and/or through inelastic deformation of erupted products and/or vent structures (McGetchin and Chouet, 1979). Calculation of the absolute acoustic and seismic efficiency, defined as the ratio of radiated elastic energy to explosive yield, is beyond the scope of this paper.

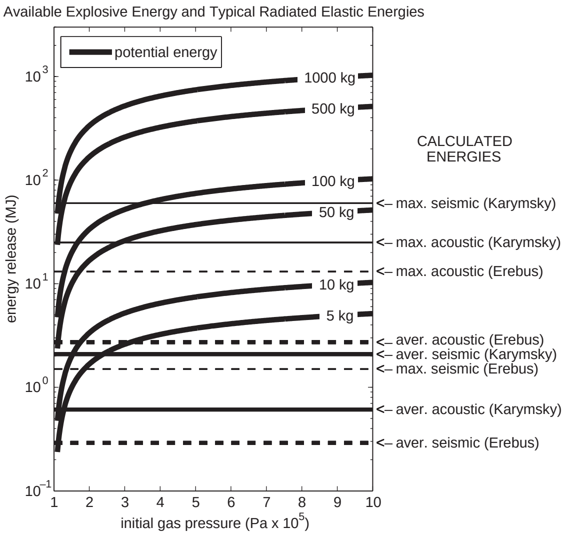

Fig. 6. Illustration of the potential energy available during gas expansion as a function of volatile mass and initial gas pressurization (thick gray lines; calculated from Eq. (4)). The estimated explosive yield for typical Strombolian events is likely to lie above the uppermost gray curve, which would correspond to explosive gas fluxes in excess of 10^3 kg (Chouet et al., 1974; Johnson, 2000). Calculated average and maximum elastic energies for discrete Erebus and Karymsky explosive events (black lines; corresponding to data shown in Fig. 5) show that potential energy transferal into the seismic and acoustic wavefield is a highly inefficient process.

In the following discussions, we make the assumption that the majority of elastic energy is radiated during individual bubble or bubble foam fragmentation processes. When bubble walls are disrupted within the melt, confining surface tension and remnant viscous overpressures are dramatically reduced (Proussevitch and Sahagian, 1996), allowing an impulsive expansion of gas and entrained particles. For an eruption source situated near the free surface, an accelerating multi-phase fluid can easily perturb the atmosphere, producing intense sonic and infrasonic disturbances (Gabrielson, 1998; Johnson, 2003; Lighthill, 1978; Ripepe and Gordeev, 1999; Yamasato, 1997). At Karymsky and Erebus we choose to attribute volcanic infrasound to this gas expansion model because eruption onset times, as determined with time-synced video, appear to coincide with the impulsive infrasound origin at the vent. However, we note that other, more complex models have been proposed to explain the production of volcanic infrasound recorded at various volcanoes. At Arenal, for instance, it has been suggested that rapid bubble coalescence, or explosions immersed within the melt, can radiate elastic waves that displace the free surface and produce low-frequency sound (Buckingham and Garces, 1996; Garces and McNutt, 1997). At Stromboli and Shishaldin, an alternative model suggests that oscillatory vibrations of bubbles rising within a magma column, or situated at the free surface, can perturb the atmosphere sufficiently to generate high-amplitude infrasound (Buckingham and Garces, 1996; Garces and McNutt, 1997; Vergniolle et al., 2004; Vergniolle and Brandeis, 1994; Vergniolle et al., 1996).

Though the corresponding seismic source is even less well understood, clear temporal correlation between the onset of short period seismicity and infrasound (Johnson and Lees, 2000; Johnson et al., 1998; Rowe et al., 2000) indicates that a simultaneous seismo-acoustic explosion source mechanism is probable. Reaction forces, which may be responsible for generating the seismic wavefield, include a thrust response due to upward mass evacuation (Brodsky et al., 1999) and/or rebound of tensional strain and gravitational collapse caused by infilling magma (Dibble, 1994). This second possible contribution to the seismic wavefield is not explicitly figured as a potential energy source in Eq. (4).

6. Mass-dependent transfer of explosive energy into acoustic energy

The hypothesis of Mori et al. (1989) for variable VASR is that dense ash-rich eruptions are associated with diminished acoustic radiation. We attempt to justify this observation by assuming that there is a quasi-linear relationship between explosive yield (compressed gas potential energy), seismic energy radiated during the eruption (as calculated by Eq. (2)), and kinetic energy of erupted products (i.e., gas, ash, and ballistics). We next show that radiated acoustic energy (as calculated by Eq. (1)) is not necessarily proportional to the kinetic energy of erupted products, because it depends upon the volumetric acceleration of the atmosphere. In linear acoustic theory, the far-field atmospheric pressure perturbations (ΔP) are proportional to the change in volumetric outflow due to an equivalent fluid injection. In the case of an acoustic monopole, the excess pressure is (Dowling, 1998; Lighthill, 1978)

$$\Delta P(r) \approx \frac{1}{r}\dot{q}(t - r/c) \tag{5}$$

where $\dot{q}$ is the rate change in volumetric flux (acceleration) in units of m^3/s^2, r is the distance from the acoustic source, and c is the sound speed.

Given a fixed explosive yield, we compare two end-member eruption models (Fig. 7A), a low-density (ρ_g), pure gas eruption and a high density (ρ_{g+c}), ash and ballistic-laden eruption. In this simplification, the multi-phase emissions, including gas and condensed phases, are assumed to behave as a well-mixed, homogeneous flow. If we consider identical integrated mass flux histories of erupted material for both types of eruptions (i.e., $M_{gas}=M_{g+c}$), then the kinetic energy history may be equivalent, but the volumetric accelerations ($\dot{q}$) and resultant excess pressure recorded at a fixed distance will be proportionately smaller for the high-density gas plume, because:

$$\frac{\Delta P_{g+c}}{\Delta P_{gas}} = \frac{\dot{q}(t - r/c)_{g+c}}{\dot{q}(t - r/c)_{gas}} \propto \frac{M_{g+c}/\rho_{g+c}}{M_{gas}/\rho_g} = \frac{\rho_g}{\rho_{g+c}} < 1 \tag{6}$$

The volume of a multi-component flow is equal to the combined volume of each individual phase, allowing us to redefine the dense plume (ρ_{g+c}) in terms of its gas and condensed phases:

$$\frac{M_g + M_c}{\rho_{g+c}} = \frac{M_g}{\rho_g} + \frac{M_c}{\rho_c} \tag{7}$$

Assuming that $M_c/\rho_c \ll M_g/\rho_g$ (i.e., the volume of the condensed phase is much less than the volume of the gas phase), we can simplify the excess pressure ratio:

$$\frac{\Delta P_{g+c}}{\Delta P_{gas}} \propto \left(1 + \frac{\rho_g}{\rho_c}\frac{M_c}{M_g}\right)\left(\frac{M_g}{M_g + M_c}\right) \approx \left(\frac{M_g}{M_g + M_c}\right) \tag{8}$$

For eruptions with equivalent kinetic energies, the corresponding acoustic energy ratio dense eruption plumes and pure gas plumes is then:

$$\frac{E_{A(g+c)}}{E_{A(gas)}} \approx \left(\frac{M_g}{M_g + M_c}\right)^2 \tag{9}$$

Photoballistic studies at Stromboli, which may be considered an analog for volcanic activity at Karymsky, give estimates of M_c on the order of 10^2 to 10^4 kg and M_g on the order of 10^3 kg for discrete events (Chouet et al., 1974; Ripepe and Gordeev, 1999). For this activity, variations in acoustic energy would vary by two orders of magnitude according to Eq. (9).

Though plume density is shown here to be inversely proportional to the volumetric perturbation of the atmosphere, it remains to be determined how an explosion source is able to accelerate its high-density and low-density components. Uniform acceleration of homogenous products is clearly an idealization that may only occur under special conditions, such as for flow in a narrow conduit where heterogeneous flow is inhibited. In this scenario, a plug of capping material, which may be massive but volumetrically insignificant, could be accelerated at the head of the expanding gas volume. Alternatively, explosive eruptions, such as those observed at Langila (Mori et al., 1989), may also be candidates for relatively uniform acceleration of ejecta if the fine-grained ash is well mixed within the eruptive column. For such ash-rich eruptions, it is possible to envision a spectrum of values for M_c/M_g, dependent upon the corresponding mass of entrained ash, that produce a range of radiated acoustic energy.

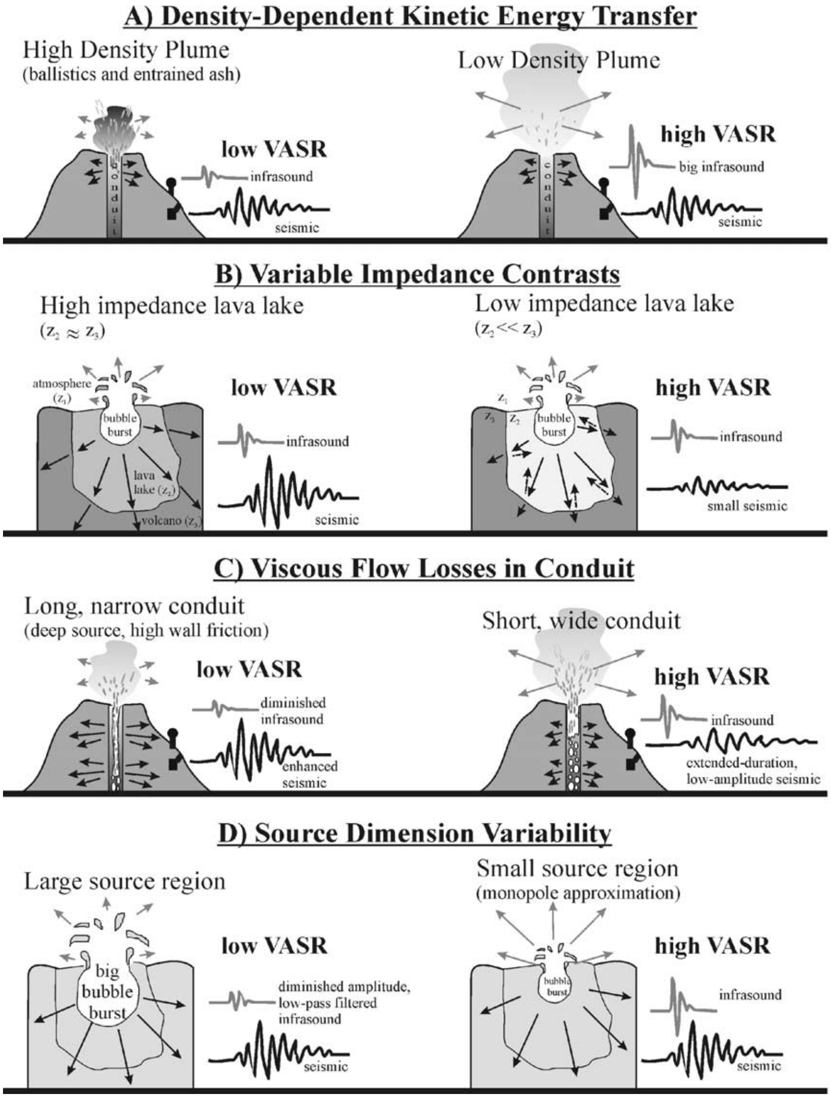

Fig. 7. Conceptualization of four important variables that may influence VASR. Gray arrows denote acoustic propagation in the atmosphere and black arrows indicate seismic propagation in the earth. Relative acoustic and seismic amplitudes are indicated. Decreased VASR might be expected for: A) dense eruption plumes, B) high lava lake magma impedance, C) deep fragmentation sources recessed within a narrow conduit, or D) large source dimension.

If seismic moment is relatively insensitive to plume density variations and is only dependent upon kinetic energy, then VASR may primarily be a function of how efficiently the atmosphere is displaced. To explain explosions with exceptionally high VASR, pressurized volatiles may expand explosively without accelerating dense cap rock or entraining much ash. This appears to be the case for explosions at the Erebus lava lake, where the rupture of a thin (<50 cm) bubble film (P. Kyle pers. comm., 2001) allows the nearly immediate and relatively unimpeded escape of pressurized gas into the atmosphere. Relatively little energy is expended in the acceleration of denser materials. Vent/conduit geometry and the overlying weight of capping material thus play a significant role in determining how dense materials and gases are preferentially accelerated.

7. Effects due to impedance contrasts

Garces and McNutt (1997) provide a formulation for the seismo-acoustic wavefield generated by a point source submerged in a conduit. Garces et al. (1998a) and Hagerty et al. (2000) utilize this foundation to explain variable seismo-acoustic energy partitioning at Arenal Volcano. Their primary thesis is that a melt-filled conduit can change from low void fraction, high impedance (acoustic velocity of ~2500 m/s) to high void fraction, low impedance (acoustic velocities < 100 m/s) over very short time intervals (Sturton and Neuberg, 2003). Assuming that associated magma densities range from 600 kg/m^3 (bubbly melt at 75% vesicularity (Sparks, 1978)) to 2500 kg/m^3 (dense magma with zero vesicularity), the acoustic impedance ($z = \rho c$) may vary by more than two orders of magnitude. While an immersed seismo-acoustic explosion source model (Garces and McNutt, 1997) and vibrating bubble modes (Vergniolle et al., 1996) are fundamentally different from the free-surface gas expansion source that is our postulated mechanism at Karymsky and that clearly occurs at Erebus (Johnson et al., 2003), changing magma impedance will still influence the relative amount of elastic energy transmitted across the conduit walls.

We address the potential effect of changing impedance contrasts by invoking a very simple plumbing geometry as an illustration (Fig. 7B). Consider an isotropic elastic radiator located at the contact between two fluid spaces (atmosphere impedance z_1 and magma impedance z_2), in which the magma volume is surrounded by solid volcano with uniform impedance z_3. For a finite explosive yield, compressional waves are propagated into the magma and atmosphere with initial intensities:

$$I_A = \frac{k_A}{2\pi\ r^2}\frac{dE_{\text{explosion}}}{dt} \tag{10}$$

$$I_S = \frac{k_S}{2\pi r^2}\frac{dE_{\text{explosion}}}{dt} \tag{11}$$

that depend upon acoustic and seismic source coupling factors (k_A and k_s). These coupling factors are functions of initial gas pressurization and density, source dimension, impedance contrasts, and other factors (Nicholls, 1962). In the interest of providing a simple and illustrative example, we assume the linear situation, where radiated elastic energy into both media is proportional to the explosive yield. Acoustic energy will then radiate through the atmosphere with minimal attenuation, dispersion, or scattering, but seismic energy imparted to the lava lake/conduit must subsequently be transmitted into the surrounding volcano. For both elastic energy and intensity (power), the P-wave transmission coefficient is at a maximum for normal incidence (Crocker, 1998).

$$T = \frac{4z_2z_3}{(z_2+z_3)^2} = \frac{4\rho_2c_2\rho_3c_3}{(\rho_2c_2+\rho_3c_3)^2} \tag{12}$$

For the range of impedances proposed by Sturton and Neuberg (2003), the maximum possible transmission coefficient ranges from near unity (for dense magma) down to a lower estimate of 10^{-3}. But at oblique incidences, such as those created by the refraction of ray paths within the strong near-surface velocity gradient of a vesiculated magma conduit (Dibble, 1994), the power transmission coefficient may be substantially reduced (Aki and Richards, 1980). Reflected elastic energy will thus tend to be trapped within the conduit/lava lake and will leak into the surrounding solid volcano only through subsequent transmissions to wall rocks and atmosphere, or be lost via intrinsic attenuation. Rowe et al. (2000) suggested that impedance isolation in the uppermost vesiculated portion of the Erebus lava lake offers an explanation for why very small bubble bursts (smaller than those observed in 1999–2000) exhibit anomalously high VASR. The hypothesis is that velocity stratification inhibits seismic energy from being transmitted to the deeper portions of the lake and/or higher impedance wall rock. Seismic wavefield calculations and simulations for a source imbedded within a fluid magma support the idea of continuing slow leakage of trapped elastic energy into the volcanic edifice (Dibble, 1994; Neuberg and O'Gorman, 2002). Together with seismic scattering in the solid media, trapped energy in the magma likely contributes to short-period seismic explosions signatures, which are greatly extended in time compared to their associated infrasound (e.g., Johnson and Lees, 2000; Rowe et al., 2000; Vergniolle and Brandeis, 1994).

Radiated seismic energy, which we measure and incorporate into our VASR calculations, will be influenced both by impedance contrasts and by attenuation characteristics of the magma. Higher attenuation, which is conceivable in gas-rich, compressible magmas (O'Connell and Budiansky, 1978), combined with severe impedance contrasts, will serve to effectively reduce the seismic energy radiated into the wall rocks. If the Erebus lava lake were composed of a frothy, low-velocity fluid, we might expect diminished seismic radiation. Although this would be a mechanism to explain the generally higher VASR observed at Erebus relative to Karymsky, there is currently no evidence to support that the Erebus phonolitic lava lake possesses lower impedance than the andesite of Karymsky.

8. Viscous flow losses

As suggested in Fig. 6, the potential energy released during 10^3 kg of gas expansion is orders of magnitude greater than the typical measured acoustic and seismic energies at Karymsky and Erebus. Though there are many possible explanations for the inefficient transferal of potential energy into elastic energy, including physical deformation of wall rock and/or non-isentropic and phase changes to the eruption products, we limit this discussion to a single type of dissipative process, energy loss due to viscous upward flow in the conduit. During an eruption, overpressure at the fragmentation depth may be substantially greater than overpressure at the vent orifice owing to a head loss within the conduit. If the orifice marks the location of the infrasound radiator, then the decrease in pressure at the vent is proportional to viscous and gravitational losses within the conduit. At the same time, turbulent conduit flow may impose stresses upon the conduit wall rock, which can contribute to the seismic wavefield in nonlinear ways (Julian, 1994). Generally, flow within a wide, smooth-walled conduit is expected to experience less viscous resistance than flow through a narrow tephra-choked conduit.

For isothermal, turbulent gas flow, the steady-state pressure gradient due to gravitational body forces and wall friction comes from the momentum equation (Fay, 1995):

$$\frac{dP}{dh} = \rho_f g - \frac{\rho_f f}{2D}\overline{V}^2 \qquad (13)$$

where ρ_f is the fluid density, g is gravity (-9.8 m s^{-2}), D is the conduit diameter, $\bar{V}$ is the average flow velocity, and f is a dimensionless frictional factor. The axis orientation (h) is defined here as positive upwards. The amount of power expended to push the fluid up through the cylindrical conduit of length *(L)* is:

$$\begin{aligned}\frac{dE_{\text{flow}}}{dt} &= \frac{dP}{dh}\left(\frac{\pi LD^2}{4}\right)\overline{V}\\ &= \left(\rho_f g - \frac{\rho_f f}{2D}V^{-2}\right)\left(\frac{\pi LD^2}{4}\right)\overline{V}\end{aligned} \qquad (14)$$

Accurate estimates of energy loss during conduit flow are difficult to evaluate from Eq. (14) because of unknown parameters, such as: ρ_f, D, $\bar{V}$, L, and especially f. Estimates of f, which depend upon the Reynold's Number of the two-phased flow and empirical coefficients, have been suggested by Dobran (1992) and Wilson (1980), but the context of these studies has typically been wide conduits (>10 m radius) with very energetic, quasi steady-state, Plinian eruptions. For flow in a cylindrical conduit with smooth walls, f may be approximated by the Darcy friction factor, which is itself dependent upon the kinematic viscosity (v) (Fay, 1995):

$$f = \frac{64v}{D\overline{V}}. \qquad (15)$$

For flow through narrow conduits with rough walls, the Darcy frictional factor will probably be insignificant compared to a wall friction term, in which case (Fay, 1995):

$$f = \frac{1}{4}\log^{-2}\left(\frac{\varepsilon/D}{3.7}\right). \qquad (16)$$

Here the wall roughness ratio (ε/D) is defined as the average dimension of protuberances (ε) divided by the conduit diameter (D).

For Karymsky-type Strombolian activity, we can very roughly estimate viscous flow losses by combining Eqs. (14) and (16). For demonstration purposes, we select a conduit diameter of 10^1 m, flow velocity of 10^2 m/s, homogeneous flow density of 10^3 kg/m^3, conduit length of 10^1 m, and wall roughness ratio of 10^{-1}. Under these flow conditions, the head loss (Eq. (13)) becomes almost equally dependent upon both viscous and gravitational terms. The expended rate of work to overcome these losses is calculated to be ~10^9 J/s, which is approximately equivalent to the explosive power produced by a 10^3 kg/s gas flux with an initial overpressure of 10^6 Pa.

This calculation suggests that it is possible for a substantial portion of the explosive yield to be dissipated before pressurized gas reaches the vent. For infrasound generated from the vicinity of the vent, the volumetric perturbation of the atmosphere and associated infrasound production may be comparably reduced. Furthermore, a portion of the energy lost during conduit flow may be transferred to the conduit walls, increasing seismic radiation. The combination of diminished acoustic efficiency and heightened seismic efficiency would thus decrease VASR.

At Karymsky, we envision that viscous dissipation during conduit flow may be quite significant given rapid flow velocities, lengthy conduits, and high wall friction factors, caused by partial conduit blockage. However, for Erebus lava lake activity the gas does not escape through conduits or cracks, and viscous wall dissipation during bubble rupture should be minimal. Individual Karymsky events, which exhibit increasing VASR through time (see Fig. 2C for an example), hint that the conduit may change (e.g., become more open) during the course of an extended period of eruptive degassing. April 1999 eruptions at Shishaldin also appeared to progress from low VASR to high VASR, consistent with vent clearing during a sub-Plinian phase (Thompson et al., 2002). These observations suggest that changing wall and conduit friction may be an important temporally evolving factor in diverse eruption situations that is easily monitored by VASR (Fig. 7C).

9. Dependence on source dimension

Idealized point sources are more efficient at radiating broadband elastic energy than dispersed source regions. In particular, high-frequency energy is inefficiently radiated for source regions comparable to, or larger than, a wavelength. Because characteristic volcanic infrasound has wavelengths that are relatively small (e.g., 340–34 m for 1–10 Hz energy) compared to characteristic seismic wavelengths (e.g., 2500–250 m for 1–10 Hz P-wave energy (Chouet et al., 1997; Dibble, 1994), a large source region could preferentially result in diminished radiated acoustic efficiency at higher frequencies. To illustrate this effect, consider a baffled circular piston of radius (a) as an acoustic radiator. In the plane of the piston surface, far-field acoustic intensity will depend upon the characteristic frequency (f) according to (Dowling, 1998):

$$I(f) = I_{\text{monopole}} \left| \frac{2J_1(2\pi af/c)}{2\pi af/c} \right|^2 \tag{17}$$

where J_1 denotes a Bessel function of the first kind. In the case of $a \to 0$, the acoustic source reduces to a monopole radiating into a halfspace. But for larger source dimensions, acoustic intensity will be diminished due to destructive interference of the higher frequency components. The band-limited (f_1, f_2) acoustic intensity for baffled pistons can be numerically calculated from Eq. (17) using

$$I(a)_{\text{piston}} = \frac{1}{f_2 - f_1} \int_{f_1}^{f2} I(f)df \tag{18}$$

For flat source spectra between 1 and 10 Hz and fixed sound speed (c=340 m/s), the acoustic efficiency, with respect to a monopole, decreases to 50% for a piston radius of 16 m, 25% for a radius of 28 m, and 10% for a radius of 51 m.

To the extent that a piston-type acoustic radiator can suitably represent certain types of volcanic eruptions, we may expect an order-of-magnitude change in radiated acoustic efficiency for very large sources (50 m as opposed to those of a few m) in the above frequency range. Other types of source geometries are also conceivable as volcanic acoustic radiators (e.g., a ring source corresponding to crater rim diffraction or line source for a fissure eruption). However, these geometries will also induce diminution in frequency-dependent acoustic efficiency comparable to the baffled piston model. Moreover, based upon visual observations, vent dimensions in excess of a few tens of meters are unlikely for the eruptive activity discussed here at either Karymsky or Erebus. Thus, order-of-magnitude variations in acoustic efficiency at Karymsky in the observed frequency band are probably not due to variable source dimensions.

10. Discussion

We propose that VASR is an easily obtained quantity with potentially significant utility for monitoring and improving understanding of key aspects of eruption dynamics. One of VASR's primary attributes is that it is a quantitative, repeatable measure of volcanic activity that is not dependent upon subjective measures of eruption magnitude for assessing changes in an erupting conduit system. In this preliminary investigation, we have identified four potential processes that are capable of influencing VASR, when considered individually. We note that changes in density-dependent mass transfer, viscous dissipation, and source dimension may affect the relative acoustic efficiency of an eruption. Similarly we have demonstrated that impedance contrasts and viscous dissipation can affect the relative seismic efficiency. In these scenarios, an increase in the relatively acoustic efficiency, without a corresponding augmentation in seismic efficiency, leads to greater VASR, whereas increased seismic efficiency without increased acoustic efficiency is linked to decreasing VASR. Based upon visual observations of a remarkably well-exposed vent system, we attribute the relatively higher VASR at Erebus to the nearly unimpeded explosive degassing that occurs at the surface of the lava lake. For Karymsky, on the other hand, we believe that relatively diminished VASR results from fragmentation sources occurring at some depth, resulting in dampened volumetric accelerations at the free surface due to viscous flow losses within a narrow, partially obstructed conduit. Evolving conduit conditions at Karymsky are likely to be controlled by the quantity of material choking the vent and/or the depth of the fragmentation source. These conditions will influence VASR and are likely changeable over short time intervals (seconds to minutes), both between individual discrete explosive events and during the course of extended-duration degassing.

For both Karymsky and Erebus, acoustic and seismic data show a substantial positive correlation between measured seismic and acoustic energy (Fig. 5), but explosive yield has a complex relation to the total radiated elastic energy and to the relative partitioning of acoustic and seismic energy. Future seismo-acoustic studies, which can integrate quantifiable observations of eruption intensity with other key observables of vent geometry and evolution (e.g., through video, gas flux, radar, or thermal studies), could contribute significantly to advancing the interpretation of VASR, and will ultimately lead to improved estimates of absolute elastic efficiencies. With proper modeling, it may then be possible to robustly estimate the magnitude of an eruption or explosive yield based upon radiated elastic energy, which remain observable even in ash-or weather-shrouded vent conditions. It may also be possible to accurately assess changing conduit conditions, source mechanisms, or magma properties based solely upon seismic and/or acoustic records.

11. Conclusion

We introduce a concept for evaluating the ratio of radiated elastic energy propagated into the atmosphere and solid earth using infrasonic pressure waveforms and seismic velocity traces. This ratio, the volcanic acoustic–seismic ratio (VASR), is an easily estimated and robust parameter for characterizing eruption sources and their elastic coupling with the volcano and atmosphere. As examples, we calculate VASR for suites of Strombolian-type explosions at Erebus and Karymsky with sensors at ranges up to several km. We show that VASR may be used to compare the changing nature of explosive eruptions from a single volcano or to intercompare eruption physics between different volcanoes.

Variable VASR at Strombolian-type systems suggests that conduit conditions vary over time as a result of elastic coupling changes with either the earth or atmosphere. If an explosion is occurring at depth within a conduit, the perturbation of the atmosphere may be appreciably reduced by viscous losses within the conduit and/or kinetic energy losses due to the fracturing of a cap rock and acceleration of denser material. A deep source may also impart correspondingly increased energy to the wall rocks and seismic wavefield through these conduit interactions, resulting in low VASR. The opposite scenario (i.e., high VASR) is expected for an unimpeded explosion occurring at, or very near, the free surface. At Karymsky we observe a large range of VASR values, hinting that conditions within the conduit are temporally variable during the observation period. At

Erebus, on the other hand, we see relatively consistent seismo-acoustic partitioning and relatively enhanced VASR. We conclude that the explanation for consistently heightened VASR at Erebus, relative to Karymsky, is the exposed, shallow location of the gas expansion source coupled with a highly repeatable eruptive process.

Acknowledgments

This research was supported by USGS Joint Operating Agreement for the Pacific Northwest Seismograph Network (PNSN; 1434-95-A-1302 and 1434-HQ-98-AG) and NSF grants (OPP-9814291, OPP-0116577, EAR-9614639, and EAR-147292). We thank the IRIS PASSCAL Instrument Center at the New Mexico Institute of Mining and Technology for essential field planning and instrumentation assistance in both Antarctica and Kamchatka. Antarctic field support was provided under the auspices of the NSF Office of Polar Programs and Raytheon Polar Services Company. We also acknowledge P. McChesney, P. Kyle, W. McIntosh, J. Lees, E. Gordeev, and M. Ripepe for essential assistance with the development, calibration, and installation of sensors in the field. We thank M. Hagerty and anonymous reviewers for suggesting substantial improvements to this manuscript.

References

Aki, K., Richards, R., 1980. Quantitative Seismology: Theory and Methods. W. H. Freeman, San Francisco. 932 pp.

Aki, K., Koyanagi, R., 1981. Deep volcanic tremor and magma ascent mechanism under Kilauea, Hawaii. J. Geophys. Res. 86 (B8), 7095–7110.

Aki, K., Ferrazzini, V., 2000. Seismic monitoring and modeling of an active volcano for prediction. J. Geophys. Res. 105, 16617–16640.

Arcineiga-Ceballos, A., Chouet, B.A., Dawson, P.B., 1999. Very long-period signals associated with vulcanian explosions at Popocatepetl Volcano, Mexico. Geophys. Res. Lett. 26, 3013–3016.

Aster, R.C., et al., 2003. Very long period oscillations of Mount Erebus Volcano. J. Geophys. Res. 108 (B11), 2522.

Battaglia, J., Aki, K., 2003. Location of seismic events and eruptive fissures on the Piton de la Fournaise volcano using seismic amplitudes. J. Geophys. Res. 108 (B8), 2364, 10.1029/2002JB002193.

Bedard, A.J., Georges, T.M., 2000. Atmospheric infrasound. Phys. Today 53 (3), 32–37.

Boatwright, J., 1980. A spectral theory for circular seismic sources: simple estimates of source dimension, dynamic stress drop, and radiated seismic energy. Bull. Seismol. Soc. Am. 70 (1), 1–27.

Brodsky, E.E., Kanamori, H., Sturtevant, B., 1999. A seismically constrained mass discharge rate for the initiation of the May 18, 1980 Mount St. Helens eruption. J. Geophys. Res. 104 (B12), 29387–29400.

Buckingham, M.J., Garces, M.A., 1996. Canonical model of volcano acoustics. J. Geophys. Res. 101 (B4), 8129–8151.

Caplan-Auerbach, J., McNutt, S.R., 2003. New insights into the 1999 eruption of Shishaldin volcano, Alaska, based on acoustic data. Bull. Volcanol. 65 (6), 405–417.

Chouet, B., Hamisevicz, N., McGetchin, T.R., 1974. Photoballistics of volcanic jet activity at Stromboli, Italy. J. Geophys. Res. 79, 4961–4976.

Chouet, B., et al., 1997. Source and path effects in the wave fields of tremor and explosions at Stromboli volcano. J. Geophys. Res. 102 (B7), 15129–15150.

Chouet, B.A., et al., 1998. Array analyses of seismic sources at Stromboli. Acta Vulcanol. 10 (2), 367–382.

Crocker, M., 1998. Introduction. In: Crocker, M. (Ed.), Handbook of Acoustics. John Wiley & Sons, New York, pp. 3–19.

Del Pezzo, E., Bianco, F., Saccorotti, G., 2001. Separation of intrinsic and scattering Q for volcanic tremor: an application to Etna and Masaya. Geophys. Res. Lett. 28, 3083–3086.

Dibble, R.R., 1994. Velocity modeling in the erupting magma column of Mount Erebus, Antarctica. In: Kyle, P.R. (Ed.), Volcanological and Environmental Studies of Mount Erebus, Antarctica. Antarctic Research Series. American Geophysical Union, pp. 17–33.

Dobran, F., 1992. Nonequilibrium flow in volcanic conduits and applications to the eruptions of Mount St. Helens on May 18, 1980, and Vesuvius in A.D. 79. J. Volcanol. Geotherm. Res. 49, 285–311.

Dobrovol'skiy, I.P., 1994. Seismic efficiency of the tectonic earthquake. Phys. Solid Earth 30 (5), 462–465.

Dowling, A.P., 1998. Steady-state radiation from sources. In: Crocker, M. (Ed.), Handbook of Acoustics. John Wiley & Sons, New York, pp. 99–117.

Duvall, W.I., Stephenson, D.E., 1965. Seismic energy available from rockbursts and underground explosions. Trans. Soc. Min. Eng. 232 (3), 235–240.

Fay, J.A., 1995. Introduction to Fluid Mechanics. MIT Press, Cambridge. 605 pp.

Fehler, M., 1983. Observations of volcanic tremor at Mount St. Helens Volcano. J. Geophys. Res. 88 (B4), 3476–3484.

Firstov, P.P., Kravchenko, N.M., 1996. Estimation of the amount of explosive gas released in volcanic eruptions using air waves. Volcanol. Seismol. 17, 547–560.

Gabrielson, T.B., 1998. Infrasound. In: Crocker, M. (Ed.), Handbook of Acoustics. John Wiley & Sons, Inc., New York.

Garces, M., 2003. pers. comm.

Garces, M.A., McNutt, S.R., 1997. Theory of the airborne sound field generated in a resonant magma conduit. J. Volcanol. Geotherm. Res. 78 (3–4), 155–178.

Garces, M.A., Hagerty, M.T., Schwartz, S.Y., 1998. Magma acoustics and time-varying melt properties at Arenal Volcano, Costa Rica. Geophys. Res. Lett. 25 (13), 2293–2296.

Garces, M.A., Hansen, R.A., Lindquist, K., 1998. Traveltimes for infrasonic waves propagating in a stratified atmosphere. Geophys. J. Int. 135 (1), 255–263.

Hagerty, M.T., Protti, M., Schwartz, S.Y., Garces, M.A., 2000. Analysis of seismic and acoustic observations at Arenal Volcano, Costa Rica, 1995–1997. J. Volcanol. Geotherm. Res. 101 (1–2), 27–65.

Hedlin, M.A.H., Berger, J., 2002. Experiments with Infrasonic Noise-Reducing Spatial Filters, 24th Seismic Research Review, pp. 783–792.

Hedlin, M.A.H., Berger, J., Vernon, F., 1999. Surveying Infrasonic Noise on Oceanic Islands, 21st Seismic Research Symposium, pp. 141–150.

Hellweg, M., 2000. Physical models for the source of Lascar's harmonic tremor. J. Volcanol. Geotherm. Res. 101 (1–2), 183–198.

Hidayat, D., Chouet, B.A., Voight, B., Dawson, P.B., Ratdomopurbo, A., 2002. Source mechanism of very-long-period signals accompanying dome growth activity at Merapi volcano, Indonesia. Geophys. Res. Lett. 29 (23), 2118–2121.

Ivanov, B.V., Braitseva, O.A., Zubin, M.I., 1991. Karymsky Volcano, Active Volcanoes of Kamchatka. Nauka, Moscow.

Johnson, J.B., 2000. Interpretation of infrasound generated by erupting volcanoes and seismo-acoustic energy partitioning during Strombolian explosions. PhD Thesis, University of Washington, Seattle, 159 pp.

Johnson, J.B., 2003. Generation and propagation of infrasonic airwaves from volcanic explosions. J. Volcanol. Geotherm. Res. 121 (1–2), 1–14.

Johnson, J.B., Lees, J.M., 2000. Plugs and chugs—seismic and acoustic observations of degassing explosions at Karymsky, Russia and Sangay, Ecuador. J. Volcanol. Geotherm. Res. 101 (1–2), 67–82.

Johnson, J.B., Lees, J.M., Gordeev, E.I., 1998. Degassing explosions at Karymsky Volcano, Kamchatka. Geophys. Res. Lett. 25 (21), 3999–4042.

Johnson, J.B., et al., 2003. Interpretation and utility of infrasonic records from erupting volcanoes. J. Volcanol. Geotherm. Res. 121 (1–2), 15–63.

Johnson, J.B., Aster, R.C., Kyle, P.R., 2004. Volcanic eruptions observed with infrasound. Geophys. Res. Lett. 31 (L14604), 10.1029/2004GL020020.

Julian, B.R., 1994. Volcanic tremor: nonlinear excitation by fluid flow. J. Geophys. Res. 99 (B6), 11859–11877.

Kinney, G.F., Graham, K.J., 1985. Explosive Shocks in Air. Springer-Verlag, New York. 269 pp.

Kyle, P., 2001. pers. comm.

Kyle, P.R., 1994. Preface. In: Kyle, P.R. (Ed.), Volcanological and Environmental Studies of Mount Erebus, Antarctica. Antarctic Research Series. American Geophysical Union, pp. 13–14.

Lighthill, M.J., 1978. Waves in Fluids. Cambridge University Press, New York. 504 pp.

McGetchin, T.R., Chouet, B.A., 1979. Energy budget of the Volcano Stromboli. Geophys. Res. Lett. 6 (4), 317–320.

McNutt, S.R., 1994. Volcanic tremor from around the world: 1992 update. Acta Vulcanol. 5, 197–200.

Metaxian, J.P., Lesage, P., Dorel, J., 1997. The permanent tremor of Masaya volcano, Nicaragua: wave field analysis and source location. J. Geophys. Res. 102, 22529–22545.

Mikumo, T., Bolt, B.A., 1985. Excitation mechanism of atmospheric pressure waves from the 1980 Mount St. Helens eruption. Geophys. J. R. Astron. Soc. 81 (2), 445–461.

Mora, M., et al., 2001. Detection of seismic site effects by using H/V spectral ratios at Arenal volcano (Costa Rica). Geophys. Res. Lett. 28, 2991–2994.

Mori, J., et al., 1989. Seismicity associated with eruptive activity at Langila Volcano, Papua New Guinea. J. Volcanol. Geotherm. Res. 38 (3–4), 243–255.

Myagkov, N.N., 1998. Model of a strong volcanic blast and a method of estimating the mass ejected. Geophys. J. Int. 133 (1), 209–211.

Neuberg, J., O'Gorman, C., 2002. A model of the seismic wavefield in gas-charged magma: application to Soufriere Hills volcano, Montserrat. In: Druitt, T.H., Kokelaar, B.P. (Eds.), The Eruption of Soufriere Hills Volcano, Montserrat, from 1995 to 1999. Geological Society of London, London, pp. 603–609.

Neuberg, J., Luckett, R., Ripepe, M., Braun, T., 1994. Highlights from a seismic broadband array on Stromboli volcano. Geophys. Res. Lett. 21 (9), 749–752.

Newhall, C.G., Self, S., 1982. The volcanic explosivity index (VEI): an estimate of explosive magnitude for historical volcanism. J. Geophys. Res. 87 (C2), 1231–1238.

Nicholls, H.R., 1962. Coupling explosive energy to rock. Geophysics 27 (3), 305–316.

O'Connell, R., Budiansky, B., 1978. Measurements of dissipation in viscoelastic media. Geophys. Res. Lett. 5 (1), 5–8.

Olson, J.V., Wilson, C.R., 1999. Simultaneous Comparison of Three Co-Located Pipe Systems for Wind-Noise Reduction for Use with Model #4 Chaparral Infrasonic Microphones at Fairbanks, Alaska, 21st Seismic Research Symposium, pp. 169–174.

Pierce, A.D., 1981. Acoustics: an introduction to its physical principles and applications. Series in Mechanical Engineering. McGraw-Hill, New York. 642 pp.

Proussevitch, A.A., Sahagian, D.L., 1996. Dynamics of coupled diffusive and decompressive bubble growth in magmatic systems. J. Geophys. Res. 101, 17156–17447.

Raspet, R., 1998. Shock waves, blast waves, and sonic booms. In: Crocker, M. (Ed.), Handbook of Acoustics. John Wiley & Sons, New York, pp. 293–303.

Reed, J.W., 1987. Air pressure waves from Mount St. Helens eruptions. J. Geophys. Res. 92 (D10), 11979–11982.

Ripepe, M., Gordeev, E.I., 1999. Gas bubble dynamics model for shallow volcanic tremor at Stromboli. J. Geophys. Res. 104 (B5), 10639–10654.

Ripepe, M., Rossi, M., Saccorotti, G., 1993. Image processing of explosive activity at Stromboli. J. Volcanol. Geotherm. Res. 54 (3–4), 335–351.

Ripepe, M., Ciliberto, S., Schiava, M.D., 2001. Time constraints for modeling source dynamics of volcanic explosions at Stromboli. J. Geophys. Res. 106 (B5), 8713–8727.

Rowe, C.A., Aster, R.C., Kyle, P.R., Schlue, J.W., Dibble, R.R., 1998. Broadband recording of Strombolian explosions and associated very-long-period seismic signals on Mount Erebus volcano, Ross Island, Antarctica. Geophys. Res. Lett. 25, 2297–2300.

Rowe, C.A., Aster, R.C., Kyle, P.R., Dibble, R.R., Schlue, J.W., 2000. Seismic and acoustic observations at Mount Erebus Volcano, Ross Island, Antarctica. J. Volcanol. Geotherm. Res. 101 (1–2), 105–128.

Ruiz, M.C., 2003. Harmonic tremor from Erebus Volcano. MS Thesis, New Mexico Institute of Mining and Technology, Socorro.

Sparks, R.S.J., 1978. The dynamics of bubble formation and growth in magmas: a review and analysis. J. Volcanol. Geotherm. Res. 3, 1–37.

Sturton, S., Neuberg, J., 2003. The effects of a decompression on seismic parameter profiles in a gas-charged magma. J. Volcanol. Geotherm. Res. 128, 187–199.

Tahira, M., Nomura, M., Sawada, Y., Kamo, K., 1996. Infrasonic and acoustic-gravity waves generated by the Mount Pinatubo eruption of June 15, 1991. In: Newhall, C.G., Punongbayan, R.S. (Eds.), Fire and Mud. University of Washington Press, Seattle, pp. 601–614.

Thompson, G., McNutt, S.R., Tytgat, G., 2002. Three distinct regimes of volcanic tremor associated with the eruption of Shishaldin Volcano, Alaska 1999. Bull. Volcanol. 64 (8), 535–547.

Vergniolle, S., Brandeis, G., 1994. Origin of sound generated by Strombolian explosions. Geophys. Res. Lett. 21 (18), 1959–1962.

Vergniolle, S., Brandeis, G., Mareschal, J.-C., 1996. Strombolian explosions 2, Eruption dynamics determined from acoustic measurements. J. Geophys. Res. 101 (B9), 20449–20466.

Vergniolle, S., Boichu, M., Caplan-Auerbach, J., 2004. Acoustic measurements of the 1999 basaltic eruption of Shishaldin volcano, Alaska: 1. Origin of Strombolian activity. J. Volcanol. Geotherm. Res. 137, 135–151.

Wilson, L., 1980. Relationships between pressure, volatile content and ejecta velocity in three types of volcanic eruptions. J. Volcanol. Geotherm. Res. 8, 297–314.

Withers, M., Aster, R., Young, C., Chael, E., 1996. High frequency analysis of seismic background and signal to noise ratio near Datil, New Mexico. Bull. Seismol. Soc. Am. 86, 1507–1515.

Woulff, G., McGetchin, T.R., 1975. Acoustic noise from volcanoes: theory and experiment. Geophys. J.R. Astr. Soc. 45, 601–616.

Yamasato, H., 1997. Quantitative analysis of pyroclastic flows using infrasonic and seismic data at Unzen Volcano, Japan. J. Phys. Earth 45, 397–416.